Title

Conjugate adaptive optics with remote focusing in multiphoton microscopy

Authors

Tao, Xiaodong
Lam, Tuwin
Zhu, Binbgzhao
et al.

Publication Date

2018-02-01

Peer reviewed

PROCEEDINGS OF SPIE

SPIEDigitalLibrary.org/conference-proceedings-of-spie

Conjugate adaptive optics with remote focusing in multiphoton microscopy

Xiaodong Tao, Tuwin Lam, Bingzhao Zhu, Qinggele Li, Marc R. Reinig, et al.

Xiaodong Tao, Tuwin Lam, Bingzhao Zhu, Qinggele Li, Marc R. Reinig, Joel Kubby, "Conjugate adaptive optics with remote focusing in multiphoton microscopy," Proc. SPIE 10502, Adaptive Optics and Wavefront Control for Biological Systems IV, 105020E (23 February 2018); doi: 10.1117/12.2292492

SPIE.

Event: SPIE BiOS, 2018, San Francisco, California, United States

Conjugate adaptive optics with remote focusing in multiphoton microscopy

Xiaodong Tao,* Tuwin Lam, Bingzhao Zhu, Qinggele Li, Marc R. Reinig, Joel Kubby
W.M. Keck Center for Adaptive Optical Microscopy, Jack Baskin School of Engineering, University of California, Santa Cruz, CA 95064, USA

ABSTRACT

The small correction volume for conventional wavefront shaping methods limits their application in biological imaging through scattering media. In this paper, we take advantage of conjugate adaptive optics (CAO) and remote focusing (CAORF) to achieve three-dimensional (3D) scanning through a scattering layer with a single correction. Our results show that the proposed system can provide 10 times wider axial field of view compared with a conventional conjugate AO system when 16,384 segments are used on a spatial light modulator. We demonstrate two-photon imaging with CAORF through mouse skull. The fluorescent microspheres embedded under the scattering layers can be clearly observed after applying the correction.

Keywords: Imaging through turbid media, Multiple scattering, Adaptive optics, Multiphoton microscopy

1. INTRODUCTION

High-resolution optical imaging through scattering media is extremely important for noninvasive biological imaging. Most optical imaging systems rely on ballistic light transmitted through a biological sample to form an image. As the imaging depth increases, multiple scattering becomes a dominant factor limiting the image depth. High-order wavefront shaping methods for compensation of scattering have been investigated extensively in recent years [1]. Recently, a conjugate AO (CAO) multiphoton system has been demonstrated for high-resolution in-vivo imaging of neurons through a mouse skull [2]. Scattering from the mouse skull is compensated by a segmented deformable mirror that is conjugated with the skull.

In this paper, we take advantage of CAO and remote focusing (CAORF) to achieve three-dimensional (3D) scanning through a scattering layer with a single correction. The axial scanning is achieved without changing the conjugation by a remote focusing (RF) module. By using a high-speed RF module, this method has the potential to extend its applications to high-speed volumetric imaging through scattering layers, such as transcranial or transcuticular functional imaging. This paper also gives thorough simulations and experimental analysis of both CAORF and the conventional CAO without RF, which shows the benefits of maintaining conjugation during axial scanning. We demonstrate two-photon imaging with CAORF through mouse skull tissue. The fluorescent microsphere embedded under the scattering layers can be clearly observed after applying the correction.

2. CONCEPT

Three configurations of the AO laser scanning systems are shown in Figs. 1(a-c). The conventional pupil AO configuration projects the phase on the SLM to the pupil plane of the objective, as shown in Fig. 1(a). The conjugate plane shifts laterally and axially during 3D scanning. This setup is efficient for compensating low-order refractive aberration, where the FOV is limited by the transverse correlation length σ_x of the distorted wavefront. For highly scattering media, where the transverse correlation length of the distorted wavefront is much smaller than the SLM segment size, this configuration gives a very limited lateral and axial FOV. The lateral FOV is determined by [3]:

$$X_{FOV} = 2\sigma_{SLM}, \tag{1}$$

where σ_{SLM} is the SLM segment size on the conjugate plane. When the scattering layer or the objective shifts along the Z-axis, Δ_Z, the segment phase on the scattering layer is rescaled along the optical axis because of the beam convergence, as shown in Fig. 1(a). The effective area in each channel for scattering compensation decreases with the axial shift. The

*xiaod.tao@gmail.com;

Adaptive Optics and Wavefront Control for Biological Systems IV, edited by Thomas G. Bifano, Joel Kubby, Sylvain Gigan, Proc. of SPIE Vol. 10502, 105020E · © 2018 SPIE ·
CCC code: 1605-7422/18/$18 · doi: 10.1117/12.2292492

ratio of the intensity at the Δ_Z plane to that at the initial conjugate plane becomes:

$$\eta_{\Delta z} = \left(\frac{\sum_n \alpha_{n,\Delta z}}{N} \right)^2, \tag{2}$$

where $\alpha_{n,\Delta Z}$ is the ratio of the effective area to the segment area at the n^{th} segment (see Appendix, A). At the conjugate plane, $\alpha_{n,\Delta Z}=1$. N is the total number of segments.

The CAO projects the SLM onto the scattering layer as shown in Fig. 1(b). It provides a wider lateral FOV, determined by the optical 'memory effect' for the speckle correlations [3]. The lateral FOV is defined by the full width at $1/e^2$ of the intensity correlation (Eq. 12), which is $X_{FOV,e2}\sim 2.686Z\lambda/\pi L$ [4]. L is the thickness of the scattering layer. Z is the distance between the scattering layer and the focal plane. However, this configuration does not maintain conjugation during axial scanning when translating the sample. The axial FOV is the same as the pupil AO system, determined by Eq. (2).

To extend the axial FOV, a new method, integrating an RF module into a CAO system, also called CAORF, is proposed as shown in Fig. 1(c). The purpose of the RF module is to shift the focal plane without moving the sample or the objective lens. This maintains the conjugation between the wavefront corrector and the scattering layer during 3D scanning. Now the axial FOV becomes [3]:

$$Z_{FOV} = 2ZX_{FOV} / D, \tag{3}$$

where D is the diameter of the beam on the scattering layer. As the equation shows, the axial FOV is not related to the SLM segment number or size. The CAORF can provide a wide-axial FOV even when a large number of segments are used. Eq. (3) does not consider the change of the effective area during 3D scanning. A more rigorous analysis can be made by numerically calculating the memory-effect intensity correlations with both lateral and axial shifts.

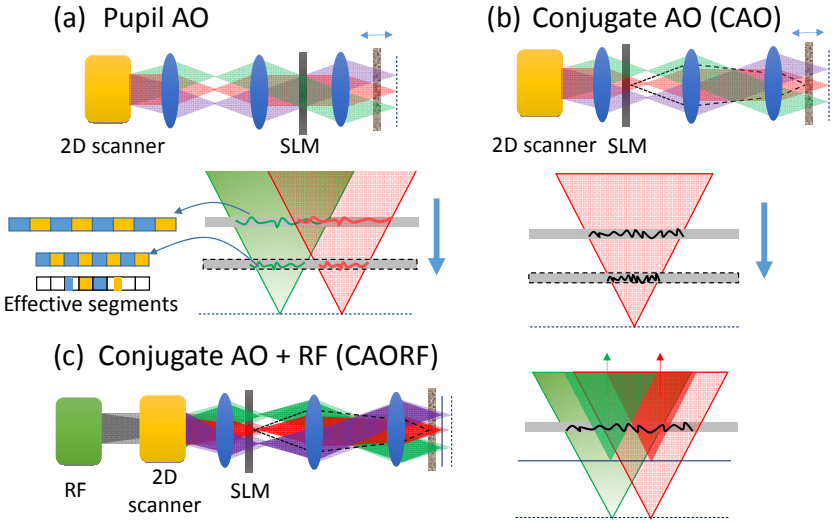

Fig 1. A schematic diagram of AO laser scanning systems. (a) Pupil AO. The SLM is conjugated with the pupil plane. The projected wavefront at the scattering layer moves with the scanning beam. The effective number of segments decreases with the axial shift. (b) Conjugate AO (CAO). The SLM is located at the plane that is conjugate to the scattering layer. The projected phase changes with the axial shift. (c) CAO and remote focusing (CAORF). The projected phase on the scattering layer does not change during three-dimensional scanning.

3. EXPERIMENTAL SETUP

Figure 2 shows the system setup to evaluate this new configuration. A solid-state laser (488 nm, LuxX 488-60, Omicron) is used as the light source for both FOV evaluation and fluorescent imaging. It is collimated by an achromatic lens L1 (f=150mm). As a proof-of-concept system, an achromatic lens L2 (f=100mm) installed on a three-axis motorized stage works as the RF and two-dimensional (2D) scanning module. Lateral scanning on the sample is realized by the translation of the lens along the X-Y axis. Translation along the Z-axis shifts the focal plane without moving the

objective lens or the sample. For real biological imaging applications, a fast 2D scanner and a RF module can be used instead. The conjugate AO module includes a reflective SLM (RCL-2500, Holoeye) and a folding mirror M1 installed on a translation stage. Lens L3 (f=100mm) and an objective lens O1 (10x, NA0.3, LEITZ) projects the phase on the SLM onto the scattering layer. The conjugation planes are aligned precisely by the translation stage without changing the final focal plane. Light from the sample is collected by another objective lens O2 (20x, NA 0.5, LEITZ) and then focused on a CCD camera (Genie M1400-1/2, Teledyne DALSA) by a lens L4 (f=150mm). For fluorescent imaging, an emission filter (FF01-542/27, Semrock) is put in the detection path, which is not shown in Fig. 2. Single sided tape (Scotch, 3M) attached on a coverslip is used as the scattering layer. The sample is mounted on a translation stage for precise adjustment. To convert the system to a two photon microscopy system, two galvanometers with relay lenses are integrated into the system to provide high-speed imaging ability as shown in Fig. 2 (b). A photomultiplier tube with additional lenses is installed near a 25x water-immersion objective (XLPLN25XWMP, NA 1.05, Olympus). A Ti: Sapphire laser (Chameleon Ultra II, Coherent) is used to generate a two-photon fluorescence signal for both phase optimization and imaging. An iterative phase optimization procedure is used to achieve an enhanced focus using the weak two-photon signal [5, 6].

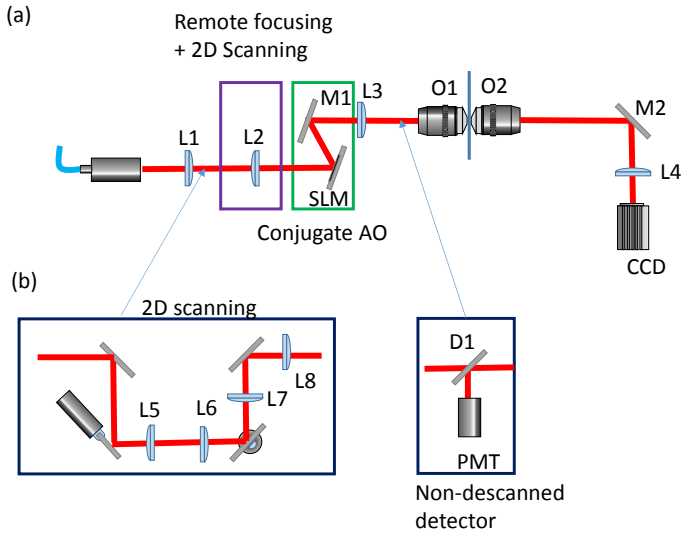

Fig. 2. System setup diagram. (a) The setup used for system evaluation. A lens (L1) collimates the laser beam from a 488nm solid-state laser. A lens (L2) installed on a three-axis translation stage works as a remote focusing (RF) and two-dimensional (2D) scanning module. The conjugate AO module consists of a spatial light modulator (SLM) and a folding mirror (M1), which are installed on a single-axis translation stage. The lens (L3) and an objective lens (O1) image the SLM plane onto the scattering layer. The light is collected by another objective lens (O2) and focused by a lens (L4) onto a CCD camera. (b) The additional modification for two-photon imaging through a mouse skull sample. Two galvanometers are used for fast scanning. L5 and L6 are relay lenses between the two scanners. Lens L7 and L8 direct the beam to the remote focusing lens (L2). A photomultiplier (PMT) and a dichroic mirror (D1) are added to the system to collect the emission light from the sample.

4. EXPERIMENTAL RESULTS

To evaluate the ability for 3D focusing through the scattering layer, a coverslip with a strip of adhesive tape is placed 2 mm from the focal plane of lens O1. Then lens O2 is moved accordingly to focus on the scattering layer. The conjugate AO module is adjusted to the conjugate plane of the scattering layer. The correct conjugation is verified by imaging both the SLM and the scattering layer on the camera. Then lens O2 is moved back to the focal plane of lens O1 to monitor the focal spot. The transmission matrix measurement is performed to generate an interferometric focus behind the scattering layer. To evaluate the focal spot in 3D space, the beam is scanned in the X-Z plane by the RF and 2D scanning modules, as shown in Fig. 3 (a). The objective lens O2 is refocused at each new depth to monitor the focus at different depths. To compare with the results without RF, the scattering layer is moved along the Z-axis as shown in Fig. 3(b). The normalized peak intensity of the focal spot along the X-Z plane with RF and without RF is shown in Fig. 3(c) and Fig. 3(d), respectively. The CAORF gives a much slower intensity drop with an axial shift in comparison to one without RF. Figure 3(e) shows the normalized peak intensity of the spot at the center of the field at different axial shifts. The red and blue dashed lines indicate the measurement data for the configurations with and without RF, respectively. The axial FOV measured by the full-width-half-maximum (FWHM) increases from 0.1 mm to 0.43 mm when RF is applied. The

simulation result is indicated by the blue line. The deviation from the experimental result are likely caused by misalignment and conjugation errors from the tilted SLM.

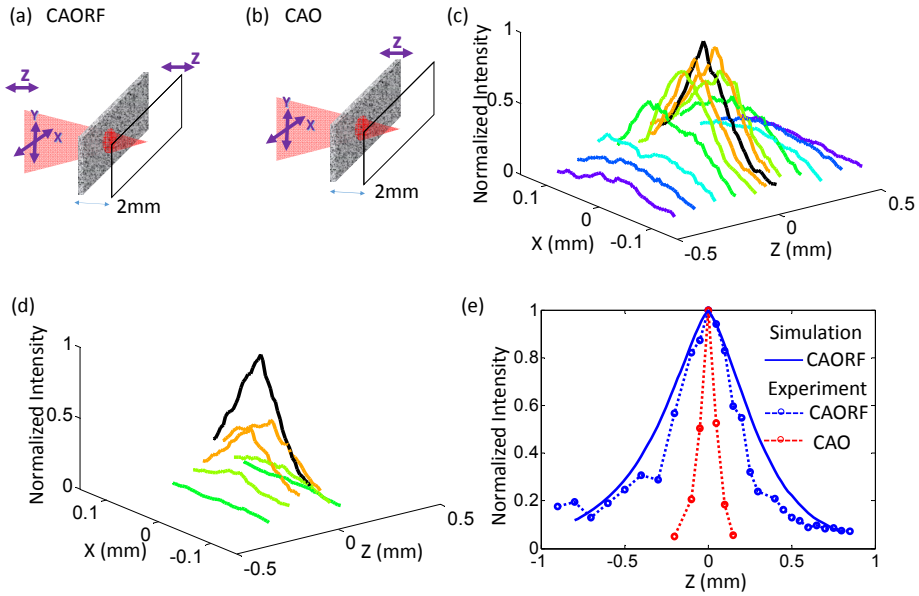

Fig. 3. Field of view analysis for 3D scanning for CAORF (a) and CAO without RF (b). The normalized intensity of the focal spot scanning along the X-Z plane for these two configurations are shown in (c) and (d), respectively. (e) The normalized intensity of the focal spot along the center of the field versus the axial shift. The red and blue dashed curves show measurement results for CAORF and CAO, respectively. The simulation of CAORF (a) is indicated by the blue curve.

Another advantage of CAORF is the insensitivity of the axial FOV to the number of segments on the SLM. A full TM is often comprised of millions of elements. Even a small fraction of the full matrix still requires thousands of channels on the SLM. For a large number of segments, the focus will be lost even with a small conjugation error caused by the focus shift. Using RF to maintain the conjugation between the SLM and the scattering layer, the axial FOV is only determined by the memory effect. Figure 4 shows the normalized intensity of the focus at various focal distances with 1024, 4096 and 16,384 segments on the SLM. The measurements with CAORF are indicated by the triangles. The results with different numbers of segments have a similar intensity drop with the axial shift, which is around 200 μm at the half-width-half-maximum (HWHM). However, without RF, the configuration with more segments gives a much smaller axial FOV. The HWHMs for 1024, 4096 and 16,384 segments drop to 40 μm, 27 μm and 19 μm, respectively. Figure 4 also shows the simulations in different situations based on Eq. 2 and Eq. 12. The difference between the measurement and simulations could be caused by the alignment error or the conjugation error from a tilted SLM. The results show the improvement of the axial FOV by 5, 7 and 10 times for 1024, 4096 and 16,384 segments, respectively.

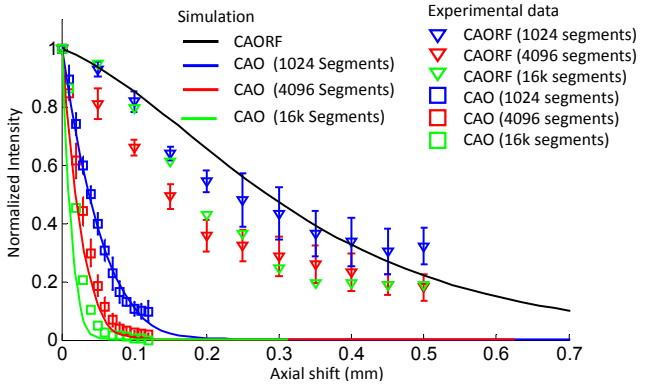

Fig. 4. Effect of the axial shift on the normalized intensity of the focal spot for different numbers of segments with CAORF and CAO. The measurements with CAORF and CAO are indicated by triangles and squares. The solid curves shows the simulation results in each case. The results for 1024, 4096 and 16,384 segments are indicated by blue, red and green, respectively.

To demonstrate the two photon imaging with CAORF, a mouse skull with a thickness of 130μm is mounted on a 170μm thick coverslip with UV-activated glue (Fotoplast Gel, Dreve, part number 44691). The scattering mean free path of the mouse skull is around 55 μm [31]. Agarose gel with 1.1 μm diameter fluorescent beads (FluoSpheres, Invitrogen) are mounted between the two coverslips. The location of the SLM is adjusted to the conjugate plane of the mouse skull. The phase optimization procedure is applied on the top surface of the agarose gel at a depth of 0μm. The laser beam is positioned at the center of the FOV, where no specific structures are apparent as shown in Fig. 5(c). After applying the final phase shown in Fig. 5(b), the microspheres can be clearly observed in Fig. 5(c). We then keep the initial phase on the SLM and shift the focal plane using the remote focusing lens (CAORF) and sample stage (CAO), respectively.

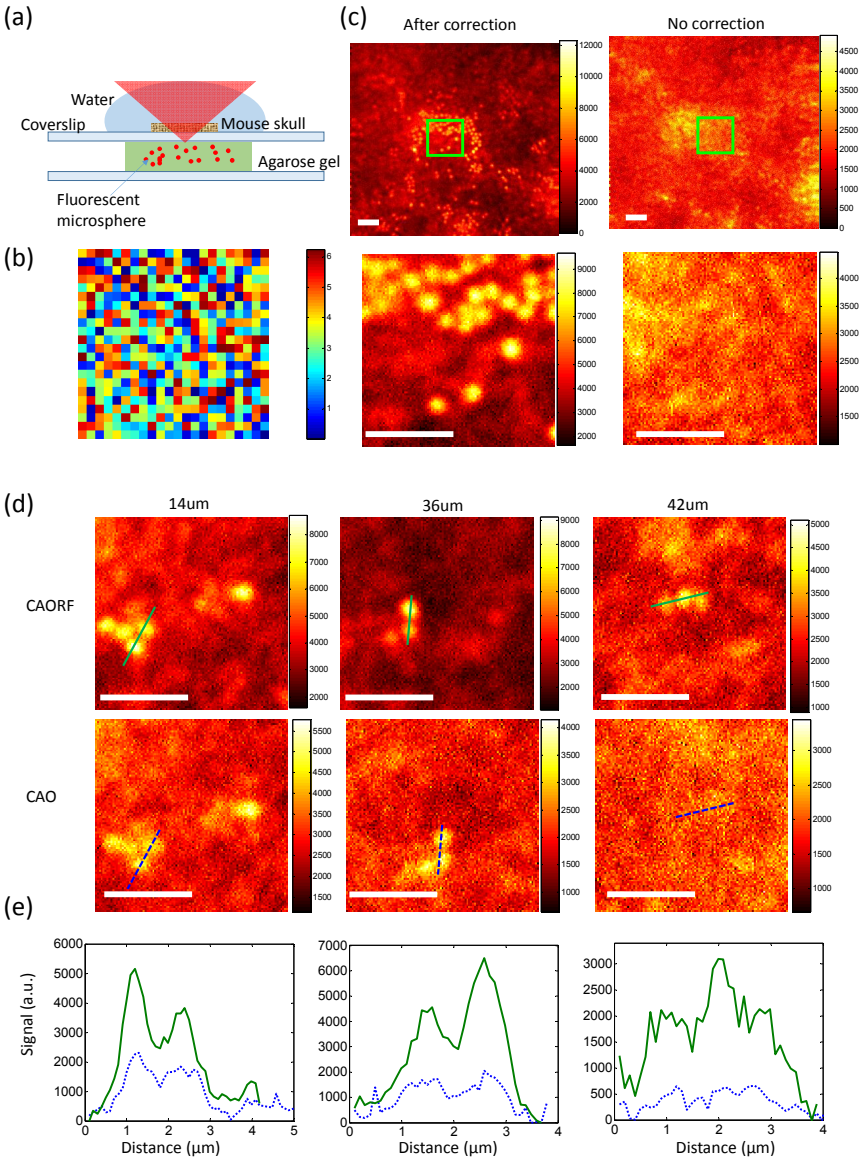

Fig. 5. Two-photon imaging of fluorescent microspheres through a mouse skull. (a) A schematic diagram of the imaging configuration. A piece of mouse skull is mounted on a 170 μm thick coverslip. Agarose gel with a thickness of 3mm is sandwiched between two coverslips. The initial correction is applied on the microspheres just below the first coverslip. (b) The phase for compensation of the scattering. (c) The images of microspheres at the top of the agarose gel (depth=0 μm) with and without correction. The green boxes indicate the enlarged view. (d) Images at depths of 14 μm, 36 μm and 42 μm with the CAORF system and the conventional CAO system. (e) The intensity profile along the line indicated in (d). The scale bar is 5 μm.

The advantages of CAORF are clearly evident in Figure 5(d) which shows comparisons of images taken at 14 μm, 36 μm and 42 μm depths for both configurations. At a depth of 42 μm, the microspheres are still observable with CAORF

but they are no longer visible with conventional CAO. Figure 5(e) shows the intensity profile along the line in Fig. 5(d). The intensity improvements are 2.2, 3.2 and 4.7 at depths of 14 μm, 36 μm and 42 μm, respectively.

5. CONCLUSIONS

In conclusion, we have demonstrated a large volume wavefront shaping method by combining CAO and RF. This configuration minimizes the conjugation error during axial scanning and provides a much larger axial FOV. Compared with a system without RF, the experiments show a 10x axial FOV improvement for 16,384 input channels on the SLM when a single layer of adhesive tape is used as a scattering layer. We have demonstrated two-photon imaging through mouse skull and showed that CAORF increases not only image quality but imaging depth in scattering biological tissue.

REFERENCES

[1] Mosk, A. P., Lagendijk, A., Lerosey, G. and Fink, M., "Controlling waves in space and time for imaging and focusing in complex media," Nat. Photonics **6**(5), 283–292 (2012).

[2] Park, J. H., Sun, W. and Cui, M. "High-resolution in vivo imaging of mouse brain through the intact skull," Proc. Natl. Acad. Sci. U.S.A. **112**(30), 9236–9241 (2015).

[3] Katz, O., Small, E. and Silberberg, Y., "Looking around corners and through thin turbid layers in real time with scattered incoherent light," Nat. Photonics **6**(8), 549–553 (2012).

[4] Schott, S., Bertolotti, J., Léger, J., Bourdieu, L. and Gigan, S. "Characterization of the angular memory effect of scattered light in biological tissues," Opt. Express **23**(10), 13505-13516 (2015).

[5] Sinefeld, D., Paudel, H. P., Ouzounov, D. G., Bifano, T. G., and Xu, C., "Adaptive optics in multiphoton microscopy: comparison of two, three and four photon fluorescence," Opt. Express **23**(24), 31472-31483 (2015).

[6] Galwaduge, P. T., Kim, S. H., Grosberg, L. E., and Hillman, E. M. C., "Simple wavefront correction framework for two-photon microscopy of in-vivo brain," Biomed. Opt. Express **6**(8), 2997-3013 (2015).